


Differential Laminar Activation Dissociates Encoding and Retrieval in the Human Medial and Lateral Entorhinal Cortex

Kaihua Zhang,^{1,2,3}  Liuyi Chen,⁴ Yinghao Li,^{2,3,5} Adrian G. Paez,^{2,3} Xinyuan Miao,^{2,3} Di Cao,^{2,3,5} Chunming Gu,^{2,3,5} James J. Pekar,^{2,3} Peter C.M. van Zijl,^{2,3} Jun Hua,^{2,3} and Arnold Bakker^{4,6}

¹School of Psychology, Shandong Normal University, Jinan 250014, China, ²F. M. Kirby Research Center for Functional Brain Imaging, Kennedy Krieger Institute, Baltimore, Maryland 21205, ³Neurosection, Division of MRI Research, Russell H. Morgan Department of Radiology and Radiological Science, Johns Hopkins University School of Medicine, Baltimore, Maryland 21287, ⁴Departments of Psychiatry and Behavioral Sciences, ⁵Biomedical Engineering, and ⁶Neurology, Johns Hopkins University School of Medicine, Baltimore, Maryland 21205

The hierarchically organized structures of the medial temporal lobe are critically important for episodic memory function. Accumulating evidence suggests dissociable information processing pathways are maintained throughout these structures including in the medial and lateral entorhinal cortex. Cortical layers provide an additional dimension of dissociation as the primary input to the hippocampus derives from layer 2 neurons in the entorhinal cortex, whereas the deeper layers primarily receive output from the hippocampus. Here, novel high-resolution T2-prepared functional MRI methods were successfully used to mitigate susceptibility artifacts typically affecting MRI signals in this region providing uniform sensitivity across the medial and lateral entorhinal cortex. During the performance of a memory task, healthy human subjects (age 25–33 years, mean age 28.2 ± 3.3 years, 4 female) showed differential functional activation in the superficial and deep layers of the entorhinal cortex associated with task-related encoding and retrieval conditions, respectively. The methods provided here offer an approach to probe layer-specific activation in normal cognition and conditions contributing to memory impairment.

Key words: 7T; cortical layer; encoding and retrieval; high field functional MRI; medial temporal lobe; T2prep

Significance Statement

This study provides new evidence for differential neuronal activation in the superficial versus deep layers of the entorhinal cortex associated with encoding and retrieval memory processes, respectively, in cognitively normal adults. The study further shows that this dissociation can be observed in both the medial and the lateral entorhinal cortex. The study was achieved by using a novel functional MRI method allowing us to measure robust functional MRI signals in both the medial and lateral entorhinal cortex that was not possible in previous studies. The methodology established here in healthy human subjects lays a solid foundation for subsequent studies investigating layer-specific and region-specific changes in the entorhinal cortex associated with memory impairment in various conditions such as Alzheimer's disease.

Received July 31, 2022; revised Feb. 28, 2023; accepted Mar. 12, 2023.

Author contributions: K.Z., L.C., A.G.P., J.H., and A.B. designed research; K.Z., Y.L., A.G.P., X.M., D.C., C.G., J.J.P., P.C.M.v.Z., J.H., and A.B. performed research; K.Z., L.C., Y.L., A.G.P., X.M., D.C., C.G., J.J.P., P.C.M.v.Z., J.H., and A.B. analyzed data; J.H., K.Z., and A.B. wrote the paper.

This work was supported by Foundation for the National Institutes of Health Grant P41 EB015909 and China Scholarship Council Grant 201806310086. We thank Joseph S. Gillen, Terri Lee Brawner, Kathleen A. Kahl, and Ivana Kusevic of the F.M. Kirby Research Center for Functional Brain Imaging at the Kennedy Krieger Institute for experimental assistance; Dr. Anne Maass for help with intersubject image alignment; Dr. Laurentius (Renzo) Huber for discussions on layer fMRI; and Dr. Ru-yuan Zhang for discussion on methods of image segmentation.

Equipment used in the study was manufactured by Philips Healthcare. P.C.M.v.Z. is a paid lecturer for Philips Healthcare and has technology licensed to Philips Healthcare. All other authors declare no competing financial interests.

Correspondence should be addressed to Jun Hua at jhua1@jhu.edu or Arnold Bakker at abakker@jhu.edu.

<https://doi.org/10.1523/JNEUROSCI.1488-22.2023>

Copyright © 2023 the authors

Introduction

The structures of the medial temporal lobe provide a hierarchical network critically important for episodic memory formation (Squire et al., 2004; Eichenbaum et al., 2007). Initial evidence from functional and anatomic studies suggested dissociable information processing pathways are maintained throughout this network differentiating spatial and nonspatial information through parahippocampal to medial entorhinal cortex (ERC) and perirhinal cortex to lateral entorhinal cortex projections. Information from both pathways is then projected to the hippocampus, thought to bind spatial and nonspatial information into a cohesive memory space (Eichenbaum, 1999; Eichenbaum et al., 1999; Davachi, 2006; Knierim et al., 2014). However, recent emerging evidence shows that the lateral

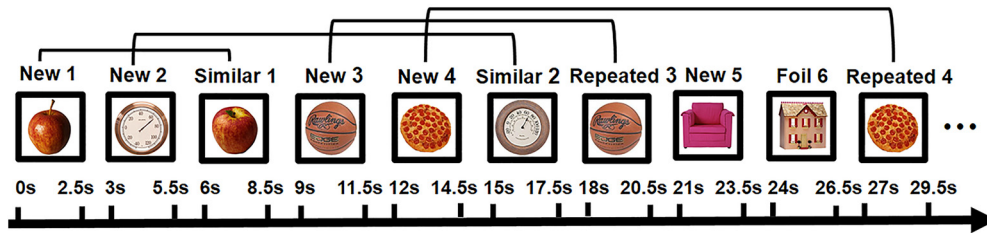


Figure 1. The memory task is designed to tax medial temporal lobe–dependent pattern separation and completion (see below, Materials and Methods). The stimuli in this task consisted of 384 pairs of color photographs of common namable objects. Ninety-six pairs consisted of identical pictures (referred to as repeated pairs), 96 pairs consisted of highly similar but not identical pictures of the same object (referred to as similar pairs), and 192 pairs consisted of unrelated single pictures of objects (referred to as foils). Stimuli were presented for 2500 ms with a 500 ms interval during which a dark screen was displayed. Illustration of the functional paradigm with examples of two pairs of repeated stimuli, two pairs of similar stimuli, and one foil stimulus are shown here. For each item, participants were asked to judge whether the item was new, old, or merely similar to an item they have seen before.

entorhinal cortex also receives input from the parahippocampal cortex suggesting it receives multimodal information and likely contributes to multiple memory processes (Doan et al., 2019; Nilssen et al., 2019). Using advances in imaging technology, previous studies have increasingly focused on subregions of the medial temporal lobe structures examining hippocampal subregion specific computations in the dentate gyrus/CA3 and CA1 (Bakker et al., 2008; Carr et al., 2010; Lacy et al., 2011; Duncan et al., 2012; Dimsdale-Zucker et al., 2018; Grande et al., 2019; Deshpande et al., 2022) and encoding of object and contextual information in the lateral and medial entorhinal cortex (Reagh and Yassa, 2014; Yeung et al., 2017; Berron et al., 2018; Reagh et al., 2018). In addition to subregions, cortical layers provide an additional dimension of dissociation as input and output of information is typically organized in different cortical layers in hierarchically organized brain systems. This is particularly prominent in the medial temporal lobes, where the primary source of input to the hippocampal formation derives from layer 2 neurons in the entorhinal cortex, and the deeper layers primarily receive output from the hippocampus (Amaral and Witter, 1989; Lavenex and Amaral, 2000; Canto et al., 2008; van Strien et al., 2009).

Blood oxygen level-dependent (BOLD) functional magnetic resonance imaging (fMRI) has enabled noninvasive examination of human brain function. As the BOLD signal shows a supralinear increase with magnetic field strength (Ogawa et al., 1993), performing BOLD fMRI at a high field strength of 7.0 tesla (7T) provides higher signal-to-noise ratio (SNR), resulting in increased sensitivity and spatial resolution (Ugurbil et al., 1993). Combined with recent advances in fast imaging and other modern MRI technologies, high-field BOLD fMRI has enabled the collection of human fMRI scans at a submillimeter spatial resolution. The distance between cortical layers associated with input and output of information typically ranges from 1 to 2 mm in many brain regions (Wagstyl et al., 2020). Thus, a submillimeter spatial resolution makes it possible to detect neuronal activation at the scale of cortical layers referred to as laminar (or layer dependent or cortical depth dependent) fMRI. Use of laminar fMRI has provided new opportunities for investigation of neuronal microcircuits in a number of brain areas, including the motor and visual cortex, and some brain regions associated with cognition (Huber et al., 2017, 2020; Finn et al., 2019, 2020). Nevertheless, well-known susceptibility artifacts (signal dropout and distortion) in conventional echoplanar imaging (EPI)-based fMRI methods makes the application of laminar fMRI in the medial temporal lobes, and specifically the entorhinal cortex, highly challenging as the ear canal adjacent to the entorhinal

cortex causes substantial artifacts that affect fMRI signals in this region (Maass et al., 2014). More importantly, the severity of such susceptibility artifacts varies across different subregions and layers in the entorhinal cortex, depending on their geometric distance and shape in relation to the adjacent ear canal. Unfortunately, these susceptibility artifacts become more prominent at higher magnetic field strengths (Ugurbil, 2013).

In an earlier study, Maass et al. (2014) used laminar fMRI at 7T and showed that processing of novel information most strongly engages the superficial layers of the entorhinal cortex as well as the dentate gyrus and CA2–3 subregions of the hippocampus, whereas the retrieval of information engaged the deeper layers of the entorhinal cortex and the pyramidal CA1 subregion of the hippocampus. A subsequent study by Koster et al. (2018) used a similar approach to examine the interaction between the layers of the entorhinal cortex and the hippocampus during inferential learning. Although dissociable activation was observed in the superficial and deep layers of the entorhinal cortex, both studies reported effects of susceptibility artifacts with ~30% of the slices obtained from the entorhinal cortex not providing usable data, especially in the lateral and anterior segments of the entorhinal cortex. Because of these artifacts, analyses were limited to the medial aspect of the entorhinal cortex as segmentations of the superficial and deep layers of the entorhinal cortex were not extended into the collateral sulcus.

T2-prepared (T2prep) BOLD fMRI is an alternative fMRI sequence developed to minimize signal loss and distortion in regions typically suffering from large susceptibility artifacts in conventional EPI-based fMRI methods (Hua et al., 2014, 2017; Miao et al., 2020). In T2prep BOLD fMRI, the BOLD contrast is generated by a T2-preparation module, followed by a readout sequence typically used in structural MRI with a much greater bandwidth compared with the EPI sequences to minimize the susceptibility artifacts. T2prep BOLD fMRI has been used in studies of healthy individuals using high-field fMRI, patients undergoing presurgical functional mapping with susceptibility artifacts of various origins, and participants with metallic dental implants (Hua et al., 2014, 2017; Miao et al., 2020) and has demonstrated significantly improved BOLD sensitivity in regions affected by large susceptibility effects compared with EPI-based fMRI methods. In this study, we performed T2prep BOLD fMRI of the medial temporal lobe at high-field (7T) strength in healthy individuals acquiring a submillimeter resolution during the performance of a memory task designed to tax encoding and retrieval functions. Although it is unlikely that computations in the entorhinal cortex layers merely reflect encoding and retrieval processes, it is a reasonable starting point to evaluate dissociable activity patterns in the deeper

versus superficial layers as well as the medial versus lateral entorhinal cortex, consistent with the approach used by Maass et al. (2014) and Koster et al. (2018). Results show that T2prep BOLD fMRI can provide consistent sensitivity across different subregions and layers in the entorhinal cortex, which enables the detection of robust laminar fMRI signals in both the medial and lateral entorhinal cortex. The used functional paradigm is designed to tax medial temporal lobe-specific functions (Fig. 1) and was used to examine whether differential functional activation associated with task-related encoding and retrieval conditions can be robustly localized to the superficial and deep layers of the entorhinal cortex with laminar fMRI at 7T.

Materials and Methods

Subjects. Ten healthy volunteers (age 25–33 years, mean age 28.2 ± 3.3 years, 4 female) participated in the current study. All participants reported being right-handed as assessed by the Edinburgh Handedness Inventory and free of major neurologic or psychiatric disorders or a history of drug or alcohol abuse. This study was approved by the Johns Hopkins Institutional Review Board. Each participant provided written informed consent before participation.

Functional paradigm. A well-established memory task designed to tax medial temporal lobe-dependent pattern separation and completion was used in this study (Kirwan and Stark, 2007; Bakker et al., 2008, 2012). The stimuli in this task consisted of 384 pairs of color photographs of common namable objects. Ninety-six pairs consisted of identical pictures (referred to as repeated pairs), 96 pairs consisted of highly similar but not identical pictures of the same object (referred to as similar pairs), and 192 pairs consisted of unrelated single pictures of objects (referred to as foils). Stimuli were presented for 2500 ms with a 500 ms interval during which a dark screen was displayed (Fig. 1). All stimuli were presented in a pseudorandom order such that paired stimuli were presented within 30 trials of its pair.

The functional paradigm was programmed using the MATLAB (MathWorks) psychophysics toolbox. The stimuli were projected from the back of the magnet onto a screen mounted on the head coil and subsequently to the center of the subjects' field of view using a custom-built mirror-prism system mounted on the head coil. Participants were instructed to press three MR-compatible response buttons to indicate whether the presented picture was new, old, or similar. One button was placed in the left hand, and two buttons were placed in the right hand. Subjects' performance during the functional memory task was assessed using their accuracy defined as the percentage of the trials within a category with correct responses. Before the MRI scan, all subjects completed a brief practice task that consisted of 96 trials outside the scanner to familiarize themselves with the stimuli and procedures. Stimuli used in the practice task were not used in the scanner task.

MRI data acquisition. All MRI scans were performed on a 7T Philips human MRI scanner (Philips Healthcare) equipped with a 32-channel phased array head coil for signal reception and an 8-channel parallel transmit head coil for transmission. To minimize subjects' head motion during the scans, custom-fit foam pads were placed around the participants' heads. An advanced B0 shim algorithm was applied using MRCODETool software (version 1.5.9, Tesla Dynamic Coils,) installed on the scanner to improve B0 field homogeneity. To improve B1 field

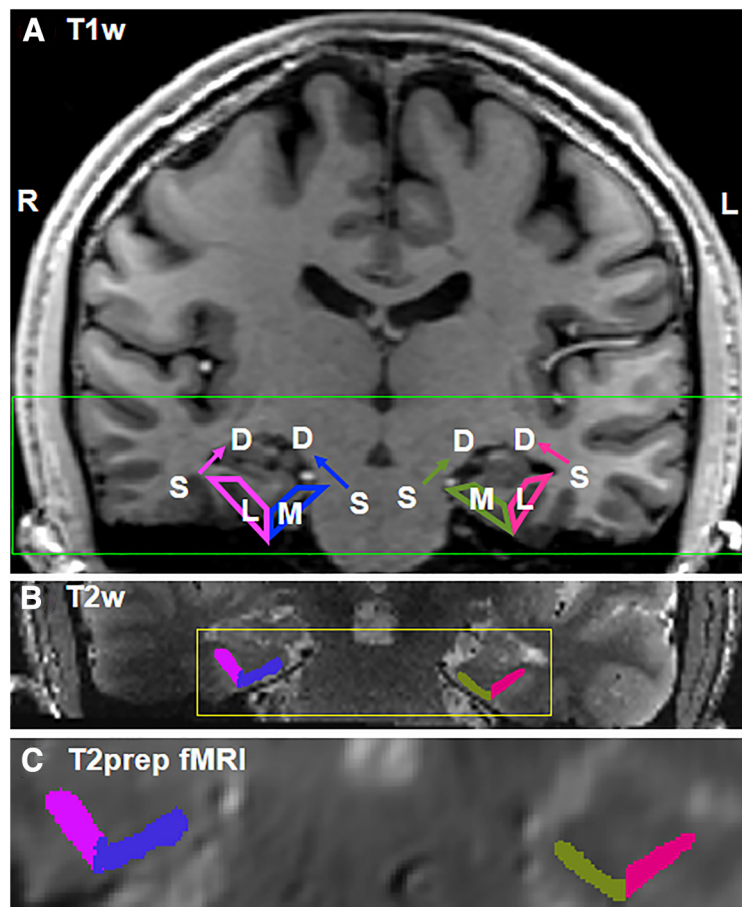


Figure 2. Segmentation of the medial and lateral components of the ERC. **A–C**, Coronal views of (**A**) T1-weighted (1 mm isotropic voxel, whole brain), (**B**) T2-weighted (0.5 mm isotropic voxel, partial brain), and (**C**) T2prep BOLD fMRI images (0.9 mm isotropic voxel, partial brain) from one representative subject are shown. The location of the medial and lateral ERC is illustrated on T1-weighted whole-brain images and the manual segmentation for this subject is shown on the T2-weighted and T2prep BOLD images. R, Right; L, left; S, superficial layer; D, deep layer; M, medial; L, lateral. The regions close to the CSF and WM are the superficial and deep layers, respectively. The green box indicates the coverage of the T2-weighted and T2prep BOLD fMRI images. The yellow box indicates the area magnified in the T2prep BOLD fMRI image.

Table 1. Summary of behavioral data in all subjects ($n = 10$)

Behavioral measures	Encoding trials	Retrieval trials	t	p
Reaction time (s)	1.0 ± 0.2	1.3 ± 0.2	-6.453	<0.01
Accuracy (%)	63 ± 13	65 ± 13	-4.331	<0.01

Summary of behavioral data.

homogeneity, rectangular pads filled with high dielectric constant materials (Teeuwisse et al., 2012) were placed on the side of the subjects' head. The following scans were performed in each subject with the same order: (1) A whole-brain structural scan was acquired for each subject using a T1-weighted magnetization prepared rapid gradient echo (GRE; MPRAGE) sequence with 192 slices, voxel = $1 \times 1 \times 1$ mm³, field of view (FOV) = 220×220 mm², repetition time (TR) = 5.0 ms, echo time (TE) = 1.81 ms, inversion time = 563 ms, duration = 2 min 15 s. (2) High-resolution fMRI images were collected using the T2prep BOLD fMRI sequence with 35 slices, voxel = $0.9 \times 0.9 \times 0.9$ mm³, FOV = 100×180 mm², TR = 3 s, TE = 50 ms, sensitivity encoding (SENSE) = 2×1.5 , first-order volume shim. The volume of this fMRI scan was carefully prescribed on the MPRAGE images to cover the medial temporal lobe bilaterally including the entorhinal cortex (see below, Results). The functional task was divided into eight runs of 4 min 48 s each, spaced with a 1 min break between runs. The total duration of the fMRI scans was 45 min 24 s. (3) High-resolution T2-weighted turbo spin echo (TSE) structural images were collected with identical coverage as the T2prep fMRI scans to

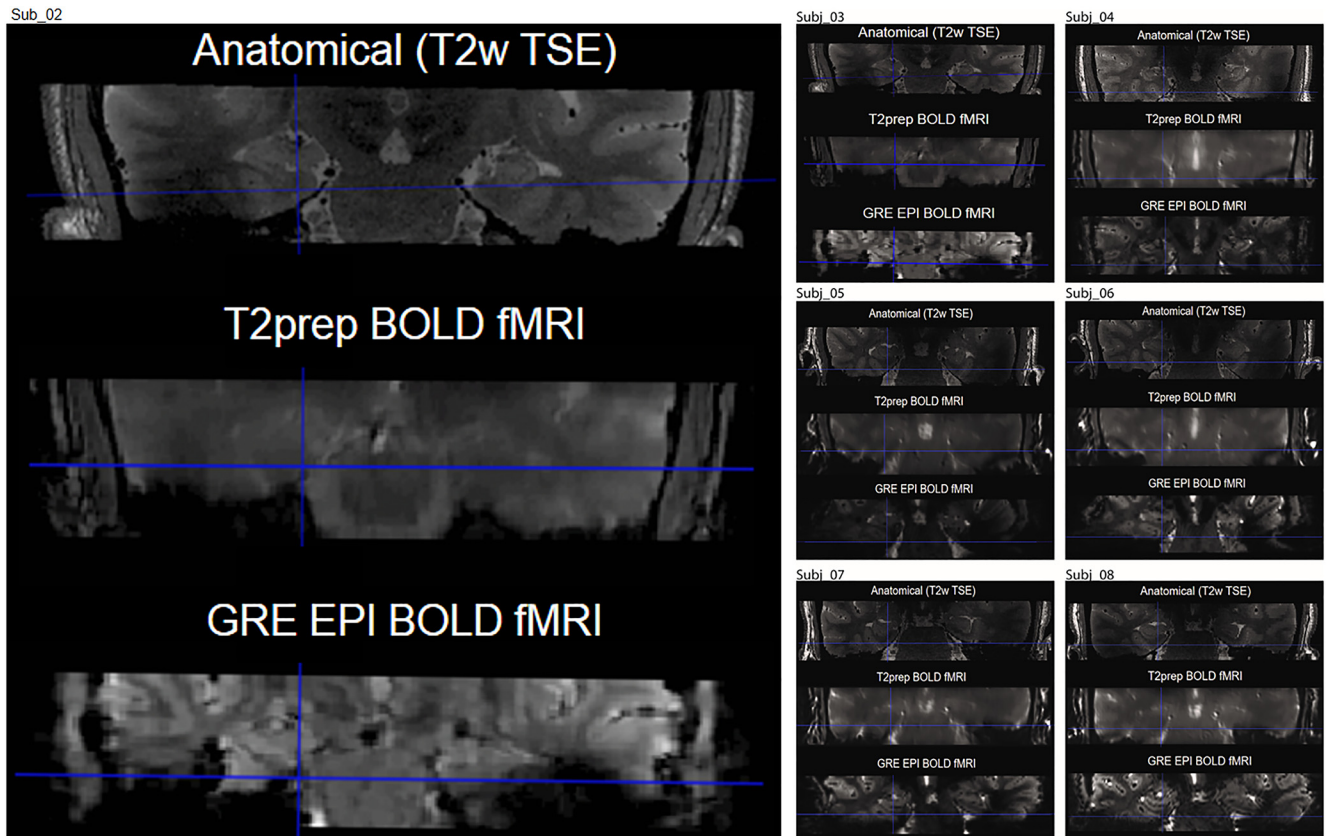


Figure 3. Representative images acquired using GRE EPI BOLD and T2prep BOLD fMRI (coronal view). In most subjects, susceptibility artifacts (signal dropout and geometric distortion caused by the nearby cavity in the ear canal) in the entorhinal cortex were significantly reduced in T2prep BOLD (middle) compared with GRE EPI BOLD (bottom). The high resolution T2-weighted image is shown as a dropout and distortion free anatomic reference (top).

allow for medial temporal lobe subfield segmentation. The following parameters were used: 70 slices, voxel size = $0.5 \times 0.5 \times 0.5 \text{ mm}^3$, TR = 5 s, TE = 57 ms, flip angle (FA) = 110° , duration = 10 min 20 s. (4) A GRE EPI BOLD fMRI scan was performed without the functional task to compare the SNR with T2prep BOLD fMRI. The following parameters were used: 35 slices, voxel = $0.9 \times 0.9 \times 0.9 \text{ mm}^3$, FOV = $100 \times 180 \text{ mm}^2$, TR = 3 s, TE = 25 ms, FA = 80° , SENSE = 3, optimal high-order shim (Schar et al., 2004), number of volumes = 20, duration = 1 min 12 s. Note that only 7 of the 10 volunteers (3 female) completed the GRE EPI BOLD fMRI scan. The total duration of all MRI scans was ~60 min.

Data analysis. Structural and functional images were analyzed using Statistical Parametric Mapping (SPM) software (Version 12, Wellcome Trust Center for Neuroimaging) and in-house programs coded in MATLAB 2018a (MathWorks). Motion correction was performed in all fMRI images using the realignment routine in SPM12 and Artifact Detection Tools (ART) software (<http://web.mit.edu/swg/software.htm>). Outlier volumes in the time series because of motion were identified and excluded using the ART toolbox based on global image intensity ($Z > 8$) and head motion ($>0.9 \text{ mm}$ translational movement in the x , y , or z plane, or $>0.03^\circ$ rotation in the yaw, pitch, or roll direction). Slice timing correction was not needed as T2prep BOLD was performed in 3D mode. To preserve the originally acquired spatial resolution in the fMRI data, no spatial smoothing was applied in the analysis. The high-resolution T2 TSE images were acquired with the same coverage as the T2prep fMRI images and were coregistered to the motion-corrected mean image from the fMRI time-series data in each subject using Advanced Normalization Tools (<https://github.com/ANTsX/ANTs>; Avants et al., 2011) and ITK-SNAP software (<http://www.itksnap.org>; Yushkevich et al., 2006). After the coregistration, Functional MRI of the Brain Software Library software (University of Oxford) was used to segment the subject-specific T2 TSE images into three tissue classes, gray matter (GM), white matter (WM), and CSF. The border lines were then manually corrected. The border lines between CSF and GM and between GM and WM were used

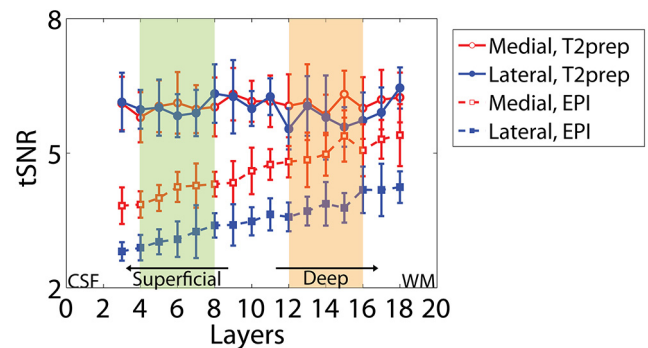


Figure 4. Average laminar tSNR profile in the lateral and medial entorhinal cortex across all subjects ($n = 7$). The x -axis shows the layer number with layers close to the CSF reflecting the superficial layers and layers close to the WM reflecting the deep layers of the entorhinal cortex. The tSNR values in the shaded layers were averaged to provide mean tSNR values in the superficial (green) and deep (orange) layers (Table 2). Error bars indicate the intersubject SEs. Data from the 1st, 2nd, 19th, and 20th layers are not shown because of the known limitation in the LayNii software for the segmentation of layers close to the rim.

Table 2. Comparison of tSNR in GRE EPI BOLD and T2prep BOLD fMRI in the entorhinal cortex ($n = 7$)

ERC	Layer	GRE EPI	T2prep	p
Medial	Superficial	4.14 ± 0.20	5.99 ± 0.12	<0.01
	Deep	5.02 ± 0.23	6.07 ± 0.17	<0.01
Lateral	Superficial	3.13 ± 0.19	6.01 ± 0.19	<0.01
	Deep	3.82 ± 0.23	5.74 ± 0.20	<0.01

Values represent mean \pm SE.

Table 3. Average head motion and outlier volumes because of excessive motion identified using the ART toolbox in each subject

Subjects	X (mm)	Y (mm)	Z (mm)	Pitch (°)	Roll (°)	Yaw (°)	Outlier volumes (trial number)
Subject 1	−0.0024	0.1040	0.1616	−0.0112	−0.0004	−0.0004	289, 576, 577, 672, 673
Subject 2	−0.3060	0.1812	−0.0991	0.0002	−0.0035	−0.0060	2, 3
Subject 3	−0.0120	−0.1252	−0.0254	−0.0107	−0.0065	−0.0017	672, 673, 674, 675
Subject 4	0.2850	0.3911	−0.3734	0.0210	−0.0100	0.0047	84, 85
Subject 5	−0.3907	0.0118	0.1119	−0.0061	−0.0020	−0.0020	192, 193, 384, 385, 576
Subject 6	0.1048	−0.1553	0.3346	−0.0181	−0.0046	0.0005	288, 289
Subject 7	0.2326	0.6104	0.3159	0.0146	0.0030	0.0004	172, 173, 174, 560, 561
Subject 8	−0.0885	0.2416	−0.2633	0.0015	−0.0068	−0.0005	96, 97
Subject 9	−0.0327	0.2538	−0.4806	0.0029	0.0016	0.0000	384, 385, 480, 481
Subject 10	−0.0205	−0.7151	−0.7898	−0.0268	−0.0023	−0.0007	678, 679

as the basis to define cortical depths. LayNii software (<https://github.com/layerfMRI/LAYNII>) was used for generating layers between these border lines (Huber et al., 2021). The layerification algorithm in LayNii was used to calculate the equidistant and equivolume metrics for each voxel between the two rims of GM (adjacent to CSF and WM, respectively) from which the desired number of layers were generated. It should be noted that layers generated by LayNii (or other similar software) are not always equivalent to histologically defined layers in neuroscience. As the typical spatial resolution used in laminar fMRI is still not sufficient to match individual biological layers, artificial layers were generated with higher resolutions than the acquired laminar fMRI images, which were then combined to match groups of biological layers of interest. The number of artificial layers was chosen based on previous laminar fMRI studies (Huber et al., 2017, 2018a,b). With a typical spatial resolution in laminar fMRI (0.6–0.9 mm) and thickness of GM (3–5 mm) in the target structure, it is recommended to extract 20 layers using LayNii (<https://layerfMRI.com/how-many-layers-should-i-reconstruct/>; Huber et al., 2017, 2018a,b). In the current study, the 20 artificial layers were later combined into two groups to investigate the superficial and deep layers in the ERC. Complete technical details on LayNii can be found in Huber et al. (2021).

The entorhinal cortex was manually delineated on the T2 TSE images in each subject and was further divided into the medial and lateral entorhinal cortex using the procedures described in Tran et al. (2021). Briefly, the entorhinal cortex was manually segmented using landmarks described by Insausti et al. (1998). The lateral boundary of the entorhinal cortex was extended to include the transentorhinal cortex, referred to as area 35 by others, given the vulnerability of this area to Alzheimer's disease (AD) pathology (Braak and Braak, 1991, 1995; Ding and Van Hoesen, 2010) while recognizing the depth of the collateral sulcus as a factor in the boundary definition at either the fundus (regular) or at the midpoint of the medial bank of the collateral sulcus (deep). The boundary between the medial and lateral segment of the entorhinal cortex was defined by drawing a vertical line down from the most inferior point of the white matter forming the medial bank of the collateral sulcus to the inferior edge of the entorhinal cortex. Manual segmentation for each subject was initiated by K.Z., and the final segmentations were completed by A.B. The segmentation of the medial and lateral ERC on representative T1-weighted, T2-weighted, and T2prep BOLD fMRI images acquired in one subject is shown in Figure 2.

A general linear model was used to detect functional activation using SPM12 in the native space. The primary contrast was constructed to compare activity during successful encoding (trials consisting of the first presentation of a repeated pair that was subsequently recognized as a

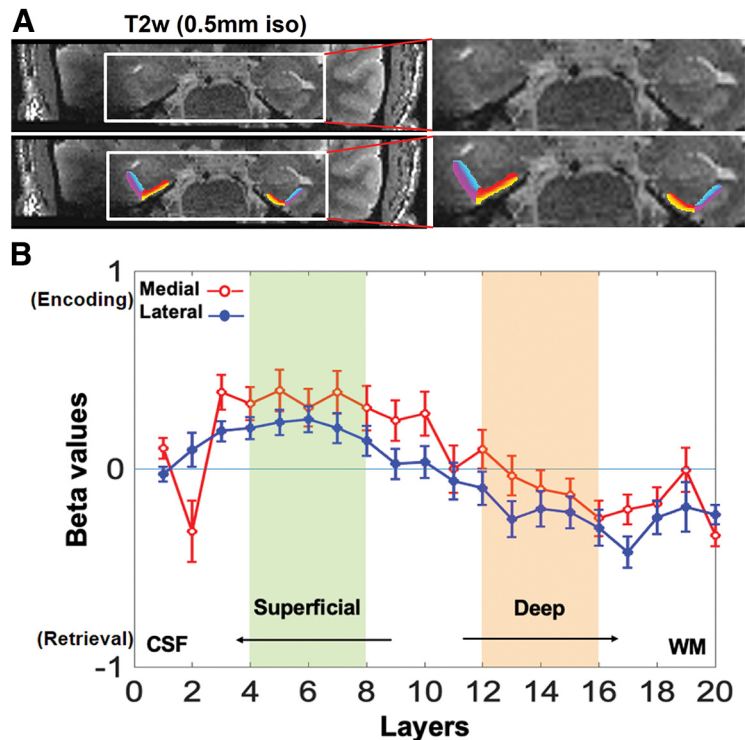


Figure 5. *A*, Top row, Representative high-resolution T2-weighted images acquired from one subject used for layer segmentation. Bottom row, The segmented superficial and deep layers in the lateral and medial entorhinal cortex are overlaid on the T2-weighted images with different colors; purple, superficial lateral; blue, deep lateral; yellow, superficial medial; red, deep medial. *B*, Mean laminar activation profile in the lateral and medial entorhinal cortex across all subjects showing activation differences between successful encoding and successful retrieval trials. Layers close to CSF and WM are superficial and deep layers, respectively. The beta values in the shaded layers were averaged to give mean activation in the superficial (green) and deep (orange) layers. Error bars indicate the intersubject SEs.

repeated picture, and trials consisting of the first presentation of a similar pair that was subsequently recognized as a similar picture) versus successful retrieval (trials consisting of the second presentation of a repeated pair that was recognized as a repeated picture, and trials consisting of the second presentation of a similar pair that was recognized as a similar picture; Kirwan and Stark, 2007; Carr et al., 2017). Additional contrasts that were evaluated include successful encoding versus foil and successful retrieval versus foil. The 3dROIstats program in Analysis of Functional NeuroImages software (National Institute of Mental Health; Cox, 1996) was used to extract specific parameters (beta values etc.) from the functional analysis. Average beta values for the superficial and deep layers were calculated using the following methods: (1) Values were averaged from the 4th to 8th layers and the 12th to 16th layers for the superficial and deep layers, respectively. The layers close to the rims were excluded because of the known limitation in the LayNii software; as the layerification in LayNii works in voxel space, based on the regular arrangement of the voxels, the layers next to the rim may be under-

represented in numbers and less reliable than other layers. (2) For all layers, the values were averaged from the 1st to 10th layers and 11th to 20th layers for the superficial and deep layers, respectively. (3) For the peak layers, they were averaged from the three consecutive layers with the most positive and most negative beta values among the 1st to 10th layers and 11th to 20th layers for the superficial and deep layers, respectively. The third method is designed to account for the potential individual differences in the structural and functional laminar profiles of the entorhinal cortex as the thickness of the layers may not always be evenly distributed, and the peak functional response may not always occur in the middle of the superficial and deep layers.

Finally, to compare the sensitivity of GRE EPI BOLD and T2prep BOLD fMRI in the entorhinal cortex, temporal SNR (tSNR) was calculated in each subject who completed both scans as the signal divided by the SD along the time course in each voxel. As only 20 dynamic scans were acquired with GRE EPI BOLD in each subject, 20 consecutive T2prep BOLD fMRI scans in the middle of the functional paradigm in each subject were chosen for the tSNR comparison.

Statistics. Statistical analysis was performed using the IBM SPSS Statistics 24.0 software. Group differences were assessed with two-tail paired *t* tests.

Data availability. Source data underlying all figures and tables in the manuscript and supplementary information are available as source data files. Additional raw images and data in this work are available from the corresponding authors on request. Correspondence and requests for materials should be addressed to the corresponding authors.

Results

Behavioral data

Mean reaction time and accuracy for the encoding and retrieval trials from all subjects are summarized in Table 1. Participants showed shorter reaction times for encoding trials compared with retrieval trials ($t = -6.453$, $p < 0.01$). The accuracy for encoding trials was significantly lower compared with the accuracy for retrieval trials ($t = -4.331$, $p < 0.01$).

Segmentation of the entorhinal cortex on structural MR images

A whole-brain T1-weighted structural MRI scan, a high-resolution fMRI scan, and a high-resolution T2-weighted structural MRI scan with identical coverage on the medial temporal lobe (Fig. 2) were collected in each participant. The entorhinal cortex was manually delineated on the T2-weighted images in each subject and was further divided into the medial and lateral entorhinal cortex using the procedures described in Tran et al. (2021; see above, Materials and Methods). The segmentation of the medial and lateral entorhinal cortex on representative T1-weighted, T2-weighted, and T2prep BOLD fMRI images acquired in one subject is shown in Figure 2.

Comparison of EPI BOLD and T2prep BOLD fMRI in the entorhinal cortex

To compare the tSNR between the conventional EPI BOLD and the T2prep BOLD fMRI approaches, a GRE EPI BOLD fMRI scan was performed in seven participants during the same MRI session. The GRE EPI BOLD images obtained from study participants showed substantial susceptibility artifacts in the entorhinal cortex. Such artifacts were significantly reduced in T2prep BOLD images from the same subjects. The individual image quality of GRE EPI BOLD and T2prep BOLD fMRI is shown in Figure 3 with the high-resolution T2-weighted images serving as an anatomic reference. The average laminar tSNR profile in the lateral and medial entorhinal cortex from all subjects is shown in Figure 4 and Table 2. In all regions T2prep BOLD showed greater tSNR when compared with GRE EPI BOLD. In GRE EPI BOLD, tSNR

Table 4. Mean beta values obtained from the contrast between successful encoding and successful retrieval trials in the medial and lateral entorhinal cortex from all subjects

Mean beta			Medial vs lateral	
	Medial ERC	Lateral ERC	<i>t</i>	<i>p</i>
Analysis method 1 (primary)				
Superficial layer	0.35 ± 0.10*	0.21 ± 0.07	1.04	0.16
Deep layer	−0.08 ± 0.09	−0.21 ± 0.09	0.97	0.18
Superficial <i>t</i>	4.18	2.10		
vs deep <i>p</i>	<0.01	0.03		
Analysis method 2				
Superficial layer	0.24 ± 0.10*	0.14 ± 0.07	0.91	0.19
Deep layer	−0.11 ± 0.09	−0.22 ± 0.09	0.80	0.22
Superficial <i>t</i>	3.00	2.32		
vs deep <i>p</i>	<0.01	0.02		
Analysis method 3				
Superficial layer	0.48 ± 0.10	0.31 ± 0.07	1.03	0.17
Deep layer	−0.33 ± 0.09	−0.47 ± 0.09	0.68	0.26
Superficial <i>t</i>	4.38	2.85		
vs deep <i>p</i>	<0.01	<0.01		

Values represent mean ± SE. The individual subject results using methods 1, 2, and 3 are provided in Extended Data Tables 4-1, 4-2, and 4-3, respectively.

was significantly smaller in the lateral entorhinal cortex compared with the medial entorhinal cortex (superficial, $t = -19.85$, $p < 0.01$; deep, $t = -21.92$, $p < 0.01$) and in superficial layers compared with deep layers (medial, $t = 17.02$, $p < 0.01$; lateral, $t = 12.99$, $p < 0.01$). In T2prep BOLD, tSNR was uniform across layers and between lateral and medial entorhinal cortex ($t = 0.14$, -0.43 , 0.87 , and -0.33 , respectively; $p > 0.1$).

Functional MRI results

The increased tSNR and signal uniformity across layers and between the lateral and medial components of the entorhinal cortex in T2prep BOLD fMRI provides validation for its use in assessing whether differential functional activation can be robustly localized to the superficial and deep layers of the entorhinal cortex in this study. Average head motion and outlier volumes excluded because of excessive motion in each subject are summarized in Table 3.

The primary contrast was constructed to compare activity during successful encoding (trials consisting of the first presentation of a repeated pair that was subsequently recognized as a repeated picture, and trials consisting of the first presentation of a similar pair that was subsequently recognized as a similar picture) versus successful retrieval (trials consisting of the second presentation of a repeated pair that was recognized as a repeated picture, and trials consisting of the second presentation of a similar pair that was recognized as a similar picture; Kirwan and Stark, 2007; Carr et al., 2017). Figure 5A shows a representative segmentation of the superficial and deep layers in the lateral and medial entorhinal cortex overlaid on high-resolution T2-weighted images. To examine differences between the superficial and deep layers of the entorhinal cortex, the mean beta values were calculated from the 4th to 8th layers and the 12th to 16th layers for the superficial and deep layers, respectively, across all subjects contrasting successful encoding and successful retrieval trials (Table 4, Fig. 5B). In both the medial and the lateral entorhinal cortex, the superficial layers showed significantly greater activation in the encoding condition compared with the retrieval condition, whereas the deep layers showed significantly greater activation in the retrieval condition compared with the encoding condition

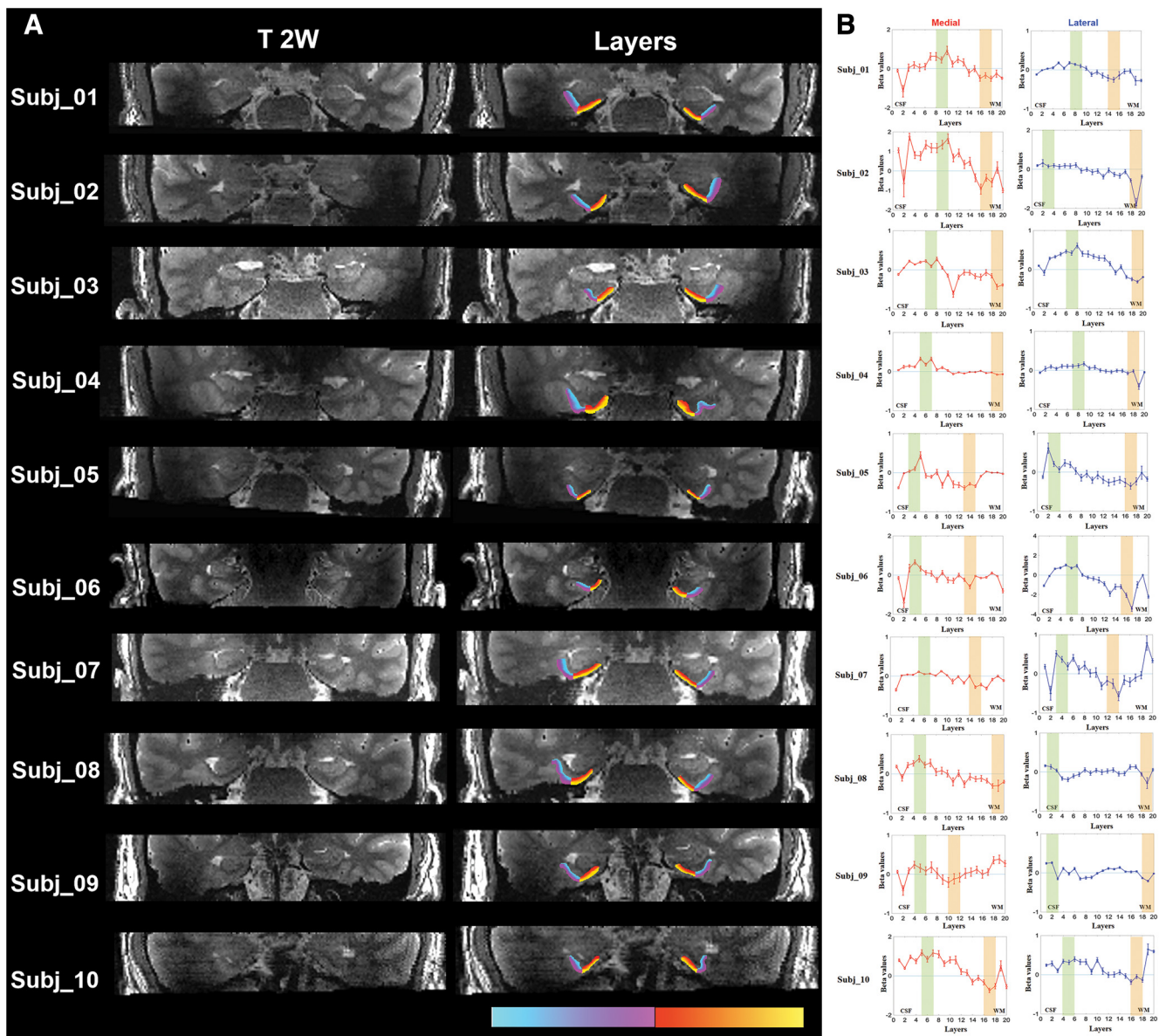


Figure 6. *A*, Left, Individual high-resolution T2-weighted images from each subject used for layer segmentation. Right, The segmented superficial and deep layers in the lateral and medial entorhinal cortex are overlaid on the T2-weighted images with different colors; purple, superficial lateral; blue, deep lateral; yellow, superficial medial; red, deep medial. *B*, Individual fMRI results and selection of layers in analysis method 3 with peak layers. The shaded areas indicate the selection of three consecutive layers with the most positive and most negative beta values among the 1st to 10th layers and the 11th to 20th layers for the superficial (green) and deep (orange) layers, respectively. The beta values in the shaded layers were averaged to give mean beta values in the superficial and deep layers, respectively. Error bars indicate the intrasubject SEs. In analysis methods 1 and 2, selection of layers is the same for all subjects (data not shown).

(medial, $t = 4.18$, $p < 0.01$; lateral, $t = 2.10$, $p = 0.03$). In the superficial layers, the magnitude of response showed a slightly greater (but nonsignificant, $t = 1.04$, $p = 0.16$) activation in the medial entorhinal cortex compared with the lateral entorhinal cortex (Table 4). In contrast, the magnitude of response in the lateral entorhinal cortex showed a slightly greater (but nonsignificant, $t = 0.97$, $p = 0.18$) activation than activity in the medial entorhinal cortex in the deep layers. The individual subject results including layer segmentation, laminar beta profiles, and average beta values in the superficial and deep layers are provided in Figure 6 and Extended Data Tables 4–2.

As the structural and functional laminar profile of the entorhinal cortex varies between individuals, the peak layers may not be identical in each subject. Therefore, the mean activation (beta) in the superficial and deep layers was additionally evaluated using

two alternative methods calculating mean activation across all layers (method 2) or from peak layers (method 3) as described above in Materials and Methods. In both methods, the superficial layers showed significantly greater activation in the encoding condition compared with the retrieval condition, whereas the deep layers showed significantly greater activation in the retrieval condition compared with the encoding condition in both the medial (method 2, $t = 3.00$, $p < 0.01$; method 3, $t = 4.38$, $p < 0.01$) and lateral entorhinal cortex (method 2, $t = 2.32$, $p = 0.02$; method 3, $t = 2.85$, $p < 0.01$). In the superficial layers, the magnitude of response showed a slightly greater (but nonsignificant, method 2, $t = 0.91$, $p = 0.19$; method 3, $t = 1.03$, $p = 0.17$) activation in the medial entorhinal cortex compared with the lateral entorhinal cortex. In contrast, the magnitude of response in the lateral entorhinal cortex showed a slightly greater (but nonsignificant,

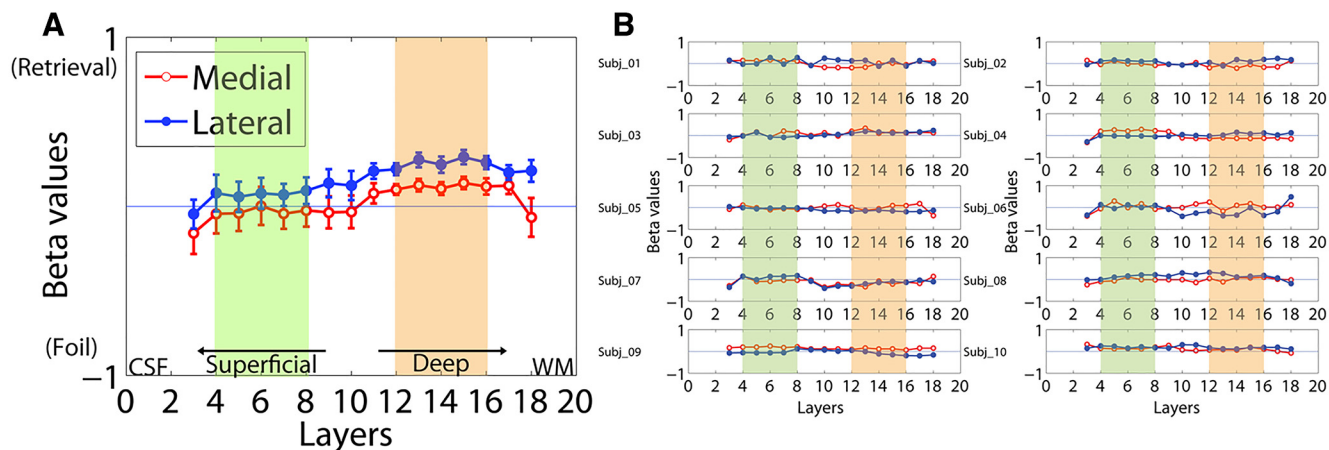


Figure 7. Laminar activation contrasting successful retrieval and successful foil trials in the lateral and medial entorhinal cortex. **A**, Mean group results. Beta values in the shaded layers were averaged to provide mean activation values in the superficial (green) and deep (orange) layers. Error bars indicate the intersubject SEs. Data from the 1st, 2nd, 19th, and 20th layers are not shown because of the known limitation in the LayNii software for the segmentation of layers close to the rim. **B**, Individual laminar beta profiles from all subjects.

Table 5. Mean beta values from the contrast between successful retrieval and foil trials in the medial and lateral entorhinal cortex

Mean beta	Medial ERC	Lateral ERC	Medial vs lateral	
			<i>t</i>	<i>p</i>
Superficial layer	-0.03 ± 0.10	0.07 ± 0.08	1.14	0.28
Deep layer	0.12 ± 0.04	0.26 ± 0.04	3.98	0.01
Superficial <i>t</i>	2.18	3.10		
vs deep <i>p</i>	0.05	0.01		

Values represent mean \pm SE.

method 2, $t = 0.80$, $p = 0.22$; method 3, $t = 0.68$, $p = 0.26$) activation than activity in the medial entorhinal cortex in the deep layers. Detailed results are provided in Figure 6B (selection of layers), Table 4 (group), and Extended Data Tables 4-2 and 4-3 (individual).

Finally, in addition to the primary contrast comparing successful encoding and successful retrieval trials, fMRI results from several other contrasts were evaluated. Comparing activation during successful retrieval and novel foil trials showed significantly increased activation in the deep layers during retrieval compared with foil trials in both the medial ($t = 2.18$, $p = 0.05$) and the lateral entorhinal cortex ($t = 3.10$, $p = 0.01$). Furthermore, activation during retrieval trials was significantly greater in the lateral entorhinal cortex than in the medial entorhinal cortex in the deep layers ($t = 3.98$, $p = 0.01$). The superficial layers did not show a significant difference in activation between the medial and the lateral entorhinal cortex ($t = 1.14$, $p = 0.28$; Fig. 7, Table 5). When evaluating the contrast between successful encoding and foil trials, no significant differences in activation were observed between the medial and lateral entorhinal cortex or between the superficial and deep layers of the entorhinal cortex.

Discussion

This study aimed to examine whether activation-associated encoding and retrieval processes can be localized to the superficial versus the deeper layers of the entorhinal cortex using laminar fMRI in human subjects. Previous studies have successfully differentiated activation in cortical layers using laminar fMRI

approaches in visual and motor cortex areas (Huber et al., 2020). Although similar approaches have been used in the entorhinal cortex (Maass et al., 2014; Koster et al., 2018), the conventional EPI-based fMRI method suffered from significant susceptibility artifacts and a drop in sensitivity in this brain region caused by the nearby ear canal, particularly in the lateral entorhinal cortex. This study used the T2prep BOLD fMRI method (Hua et al., 2014), which was developed to minimize susceptibility artifacts commonly seen in conventional EPI-based fMRI methods in regions adjacent to air cavities, bone structures, metallic implants (Miao et al., 2020), calcified structures, and hemorrhages (Hua et al., 2017). Images obtained with T2prep BOLD fMRI showed a relatively uniform laminar tSNR profile across the layers as well as the lateral and medial portions of the entorhinal cortex, whereas tSNR in GRE EPI BOLD fMRI showed a significant reduction in the superficial layers and in the lateral entorhinal cortex. Examining activation associated with encoding and retrieval processes showed a dissociation between the superficial and deep layers of the entorhinal cortex with successful encoding showing significantly greater activation in the superficial layers of both the lateral and the medial entorhinal cortex compared with the deeper layers, whereas successful retrieval processes showed significantly greater activation in the deeper layers of both the lateral and the medial entorhinal cortex compared with the superficial layers. An analysis of activation during memory retrieval compared with foil trials also showed significantly greater activation in the deeper layers of both the lateral and the medial entorhinal cortex compared with the superficial layers. In addition, this analysis showed a dissociation between activation in the lateral versus the medial entorhinal cortex with activation during memory retrieval showing significantly greater activation in the deeper layers of the lateral entorhinal cortex compared with the deeper layers of the medial entorhinal cortex. The current findings are consistent with prior reports of encoding-related activation localized to the superficial layers of the entorhinal cortex and retrieval-related activation localized to the deeper layers of the entorhinal cortex (Maass et al., 2014; Koster et al., 2018) and extend those findings to the lateral entorhinal cortex region in the collateral sulcus where traditional EPI methods resulted in significant susceptibility artifacts and signal dropout.

The landmarks used in this study are based on boundary definitions provided by Insausti et al. (1998). This approach includes part of the perirhinal cortex, referred to as the transentorhinal

cortex (Braak and Braak, 1995) or area 35 (Ding and Van Hoesen, 2010) laterally and limits the variability in individual subject segmentations that arises from individual differences in the depth of the collateral sulcus. An alternative approach is provided in the study by Maass et al. (2015) in which an analysis of functional connectivity was used to generate an anterolateral to posterior-medial dissociation in the entorhinal cortex, which showed an association with object versus spatial information processing, respectively. Their results show that in addition to a lateral and medial distinction in the entorhinal cortex, a dissociation in the anterior–posterior axis must also be considered. This approach was not used in the Maass et al. (2014) study, where the lateral boundary of the entorhinal cortex was defined by the opening of the collateral sulcus, and the segment of the entorhinal cortex located on the medial bank of the collateral sulcus was excluded because of significant susceptibility artifacts in this region. A consensus of landmarks and terminology will need to be established based on both anatomic and functional studies to further assess the functional significance of these subregions in memory function. The landmarks used here provide a reasonable demarcation to examine whether robust dissociations could be observed between the superficial and deeper layers of the entorhinal cortex as well as the medial and lateral subregions of the entorhinal cortex and particularly the component to the lateral entorhinal cortex that extends into the collateral sulcus given the technical challenges of fMRI signal acquisition in this region.

The findings in this study were observed in the context of a task designed to tax hippocampal function using objects of varying similarity. Trials were organized to reflect encoding and retrieval conditions consistent with the anatomic projections to and from both the lateral and medial entorhinal cortex and previous reports of entorhinal cortex layer-specific activation (Maass et al., 2014; Koster et al., 2018). However, previous studies have reported a functional distinction for the medial and lateral subregions of the entorhinal cortex. There appears to be a preference for allocentric spatial information in the parahippocampal to medial entorhinal cortex to proximal subiculum pathway, whereas in contrast, the perirhinal to lateral entorhinal to distal subiculum pathway demonstrates limited spatial specificity but strong involvement in processing of items and events among other contextual information (Davachi, 2006; Deshmukh et al., 2012; Knierim, 2015; Lee et al., 2020). Therefore, the absence of an observed difference in laminar activation in the medial entorhinal cortex could be the result of a lack of sensitivity of the task in the spatial domain. Additional studies using task conditions that included object identity and spatial or context processing and particularly the conjunctive encoding of an object within a context are needed to further examine layer-specific activation in the entorhinal cortex. Furthermore, although encoding and retrieval processes provide a reasonable approach to examine input from the superficial layers and output to the deeper layers of the entorhinal cortex, it is unlikely that computations in these layers merely reflect encoding and retrieval processes, particularly given the extensive associative connectivity between the layers of the entorhinal cortex and exceptions to this input and output connectivity profile (Witter and Moser, 2006; Koganezawa et al., 2008). Layer-specific activation in the entorhinal cortex should therefore additionally be examined in the context of computations and representations relevant to memory functioning in this region (Brunec et al., 2020).

The use of T2prep BOLD fMRI in this study enabled the examination of layer-specific activation in both the medial and lateral entorhinal cortex obtaining robust task-related activation

from both subregions and extending into the collateral sulcus. The examination of the lateral entorhinal cortex is of particular relevance to the study of AD, where the earliest pathologic changes are observed in the entorhinal cortex including the accumulation of tau neurofibrillary tangles (Braak and Braak, 1991) and frank neuronal degeneration and loss (Van Hoesen et al., 1991; Gómez-Isla et al., 1996; Kordower et al., 2001; Price et al., 2001). Emerging evidence further suggests that the lateral entorhinal cortex including the transentorhinal cortex may be affected earlier in the disease trajectory. In addition, neuronal hyperactivity in the hippocampus associated with memory impairment observed early in this condition (Yassa et al., 2010; Bakker et al., 2012, 2015) occurs in the CA3 and dentate gyrus subregions of the hippocampus, which receive their major cortical input from the layer 2 neurons of the entorhinal cortex. In animal models of AD, reduced reelin expression specific to the lateral entorhinal cortex has been demonstrated and reported to accelerate pathology accumulation in the medial temporal lobe. Future studies examining the functional consequence of early pathology accumulation in the superficial layers of the lateral entorhinal cortex will be key in understanding the progression of AD-related memory impairment. The methods used here provide a robust approach to examine such layer- and subregion-specific processes in AD and other conditions.

The results from the current study should be interpreted in the light of several technical limitations. First, the T2prep BOLD fMRI approach was designed to minimize the signal dropout and geometric distortion in regions affected by large susceptibility artifacts. However, the T2-weighted contrast in T2prep BOLD is less sensitive to the BOLD effect and often provides less contrast among GM, WM, and CSF, compared with the T2*-weighted contrast in conventional GRE EPI BOLD (Hua et al., 2014, 2017; Miao et al., 2020). Therefore, in regions that are less affected by susceptibility artifacts such as the visual or motor cortex, GRE EPI BOLD fMRI is still the preferred method. Second, only 10 healthy volunteers were studied, which is a small sample size. Follow-up studies with a much larger cohort are warranted to replicate and validate the current findings.

Conclusions

Differential functional activations in the superficial and deep layers and in the lateral and medial portions of the entorhinal cortex were detected using laminar fMRI performed at 7T in healthy subjects. The well-known susceptibility artifacts especially in the lateral entorhinal cortex were mitigated using an alternative T2prep BOLD fMRI approach, which showed a uniform tSNR profile across layers and subregions in the entorhinal cortex. The methodology established in the current study may offer a useful tool to probe layer-specific changes in the memory circuit in disorders such as Alzheimer's disease and Parkinson's disease.

References

- Amaral DG, Witter MP (1989) The three-dimensional organization of the hippocampal formation: a review of anatomical data. *Neuroscience* 31:571–591.
- Avants BB, Tustison NJ, Song G, Cook PA, Klein A, Gee JC (2011) A reproducible evaluation of ANTs similarity metric performance in brain image registration. *Neuroimage* 54:2033–2044.
- Bakker A, Kirwan CB, Miller M, Stark CE (2008) Pattern separation in the human hippocampal CA3 and dentate gyrus. *Science* 319:1640–1642.
- Bakker A, Krauss GL, Albert MS, Speck CL, Jones LR, Stark CE, Yassa MA, Bassett SS, Shelton AL, Gallagher M (2012) Reduction of hippocampal

- hyperactivity improves cognition in amnesic mild cognitive impairment. *Neuron* 74:467–474.
- Bakker A, Albert MS, Krauss G, Speck CL, Gallagher M (2015) Response of the medial temporal lobe network in amnesic mild cognitive impairment to therapeutic intervention assessed by fMRI and memory task performance. *Neuroimage Clin* 7:688–698.
- Berron D, Neumann K, Maass A, Schütze H, Fliessbach K, Kiven V, Jessen F, Sauvage M, Kumaran D, Düzel E (2018) Age-related functional changes in domain-specific medial temporal lobe pathways. *Neurobiol Aging* 65:86–97.
- Braak H, Braak E (1991) Neuropathological staging of Alzheimer-related changes. *Acta Neuropathol* 82:239–259.
- Braak H, Braak E (1995) Staging of Alzheimer's disease-related neurofibrillary changes. *Neurobiol Aging* 16:271–278.
- Brunec IK, Robin J, Olsen RK, Moscovitch M, Barense MD (2020) Integration and differentiation of hippocampal memory traces. *Neurosci Biobehav Rev* 118:196–208.
- Canto CB, Wouterlood FG, Witter MP (2008) What does the anatomical organization of the entorhinal cortex tell us? *Neural Plast* 2008:381243.
- Carr VA, Viskontas IV, Engel SA, Knowlton BJ (2010) Neural activity in the hippocampus and perirhinal cortex during encoding is associated with the durability of episodic memory. *J Cogn Neurosci* 22:2652–2662.
- Carr VA, Bernstein JD, Favila SE, Rutt BK, Kerchner GA, Wagner AD (2017) Individual differences in associative memory among older adults explained by hippocampal subfield structure and function. *Proc Natl Acad Sci U S A* 114:12075–12080.
- Cox RW (1996) AFNI: software for analysis and visualization of functional magnetic resonance neuroimages. *Comput Biomed Res* 29:162–173.
- Davachi L (2006) Item, context and relational episodic encoding in humans. *Curr Opin Neurobiol* 16:693–700.
- Deshmukh SS, Johnson JL, Knierim JJ (2012) Perirhinal cortex represents nonspatial, but not spatial, information in rats foraging in the presence of objects: comparison with lateral entorhinal cortex. *Hippocampus* 22:2045–2058.
- Deshpande G, Zhao X, Robinson J (2022) Functional parcellation of the hippocampus based on its layer-specific connectivity with default mode and dorsal attention networks. *Neuroimage* 254:119078.
- Dimsdale-Zucker HR, Ritchey M, Ekstrom AD, Yonelinas AP, Ranganath C (2018) CA1 and CA3 differentially support spontaneous retrieval of episodic contexts within human hippocampal subfields. *Nat Commun* 9:294.
- Ding SL, Van Hoesen GW (2010) Borders, extent, and topography of human perirhinal cortex as revealed using multiple modern neuroanatomical and pathological markers. *Hum Brain Mapp* 31:1359–1379.
- Doan TP, Lagartos-Donate MJ, Nilssen ES, Ohara S, Witter MP (2019) Convergent projections from perirhinal and postrhinal cortices suggest a multisensory nature of lateral, but not medial, entorhinal cortex. *Cell Rep* 29:617–627.e7.
- Duncan K, Ketz N, Inati SJ, Davachi L (2012) Evidence for area CA1 as a match/mismatch detector: a high-resolution fMRI study of the human hippocampus. *Hippocampus* 22:389–398.
- Eichenbaum H (1999) The hippocampus and mechanisms of declarative memory. *Behav Brain Res* 103:123–133.
- Eichenbaum H, Dudchenko P, Wood E, Shapiro M, Tanila H (1999) The hippocampus, memory, and place cells: is it spatial memory or a memory space? *Neuron* 23:209–226.
- Eichenbaum H, Yonelinas AP, Ranganath C (2007) The medial temporal lobe and recognition memory. *Annu Rev Neurosci* 30:123–152.
- Finn ES, Huber L, Jangraw DC, Molfese PJ, Bandettini PA (2019) Layer-dependent activity in human prefrontal cortex during working memory. *Nat Neurosci* 22:1687–1695.
- Finn ES, Huber L, Bandettini PA (2020) Higher and deeper: bringing layer fMRI to association cortex. *Prog Neurobiol* 207:101930.
- Gómez-Isla T, Price JL, McKeel DW Jr, Morris JC, Growdon JH, Hyman BT (1996) Profound loss of layer II entorhinal cortex neurons occurs in very mild Alzheimer's disease. *J Neurosci* 16:4491–4500.
- Grande X, Berron D, Horner AJ, Bisby JA, Düzel E, Burgess N (2019) Holistic recollection via pattern completion involves hippocampal subfield CA3. *J Neurosci* 39:8100–8111.
- Hua J, Qin Q, van Zijl PCMV, Pekar JJ, Jones CK (2014) Whole-brain three-dimensional T2-weighted BOLD functional magnetic resonance imaging at 7 Tesla. *Magn Reson Med* 72:1530–1540.
- Hua J, Miao X, Agarwal S, Bettgowda C, Quioñes-Hinojosa A, Lateral J, Zijl PCMV, Pekar JJ, Pillai JJ (2017) Language mapping using T2-prepared BOLD functional MRI in the presence of large susceptibility artifacts—initial results in patients with brain tumor and epilepsy. *Tomography* 3:105–113.
- Huber L, Handwerker DA, Jangraw DC, Chen G, Hall A, Stüber C, Gonzalez-Castillo J, Ivanov D, Marrett S, Guidi M, Goense J, Poser BA, Bandettini PA (2017) High-resolution CBV-fMRI allows mapping of laminar activity and connectivity of cortical input and output in human M1. *Neuron* 96:1253–1263.e7.
- Huber L, Ivanov D, Handwerker DA, Marrett S, Guidi M, Uludağ K, Bandettini PA, Poser BA (2018a) Techniques for blood volume fMRI with VASO: from low-resolution mapping towards sub-millimeter layer-dependent applications. *Neuroimage* 164:131–143.
- Huber L, Tse DHY, Wiggins CJ, Uludağ K, Kashyap S, Jangraw DC, Bandettini PA, Poser BA, Ivanov D (2018b) Ultra-high resolution blood volume fMRI and BOLD fMRI in humans at 9.4 T: capabilities and challenges. *Neuroimage* 178:769–779.
- Huber L, Finn ES, Chai Y, Goebel R, Stirnberg R, Stöcker T, Marrett S, Uludağ K, Kim SG, Han S, Bandettini PA, Poser BA (2020) Layer-dependent functional connectivity methods. *Prog Neurobiol* 207:101835.
- Huber LR, Poser BA, Bandettini PA, Arora K, Wagstyl K, Cho S, Goense J, Nothnagel N, Morgan AT, van den Hurk J, Müller AK, Reynolds RC, Glen DR, Goebel R, Gulban OF (2021) LayNii: a software suite for layer-fMRI. *Neuroimage* 237:118091.
- Insausti R, Juottonen K, Soininen H, Insausti AM, Partanen K, Vainio P, Laakso MP, Pitkanen A (1998) MR volumetric analysis of the human entorhinal, perirhinal, and temporopolar cortices. *AJNR Am J Neuroradiol* 19:659–671.
- Kirwan CB, Stark CE (2007) Overcoming interference: an fMRI investigation of pattern separation in the medial temporal lobe. *Learn Mem* 14:625–633.
- Knierim JJ (2015) From the GPS to HM: place cells, grid cells, and memory. *Hippocampus* 25:719–725.
- Knierim JJ, Neunuebel JP, Deshmukh SS (2014) Functional correlates of the lateral and medial entorhinal cortex: objects, path integration and local-global reference frames. *Philos Trans R Soc Lond B Biol Sci* 369:20130369.
- Koganezawa N, Taguchi A, Tominaga T, Ohara S, Tsutsui K, Witter MP, Iijima T (2008) Significance of the deep layers of entorhinal cortex for transfer of both perirhinal and amygdala inputs to the hippocampus. *Neurosci Res* 61:172–181.
- Kordower JH, Chu Y, Stebbins GT, DeKosky ST, Cochran EJ, Bennett D, Mufson EJ (2001) Loss and atrophy of layer II entorhinal cortex neurons in elderly people with mild cognitive impairment. *Ann Neurol* 49:202–213.
- Koster R, Chadwick MJ, Chen Y, Berron D, Banino A, Düzel E, Hassabis D, Kumaran D (2018) Big-loop recurrence within the hippocampal system supports integration of information across episodes. *Neuron* 99:1342–1354.e6.
- Lacy JW, Yassa MA, Stark SM, Muftuler LT, Stark CE (2011) Distinct pattern separation related transfer functions in human CA3/dentate and CA1 revealed using high-resolution fMRI and variable mnemonic similarity. *Learn Mem* 18:15–18.
- Lavenex P, Amaral DG (2000) Hippocampal-neocortical interaction: a hierarchy of associativity. *Hippocampus* 10:420–430.
- Lee H, GoodSmith D, Knierim JJ (2020) Parallel processing streams in the hippocampus. *Curr Opin Neurobiol* 64:127–134.
- Maass A, Schütze H, Speck O, Yonelinas A, Tempelmann C, Heinze HJ, Berron D, Cardenas-Blanco A, Brodersen KH, Stephan KE, Düzel E (2014) Laminar activity in the hippocampus and entorhinal cortex related to novelty and episodic encoding. *Nature Commun* 5:5547.
- Maass A, Berron D, Libby LA, Ranganath C, Düzel E (2015) Functional subregions of the human entorhinal cortex. *Elife* 4:e06426.
- Miao X, Wu Y, Liu D, Jiang H, Woods D, Stern MT, Blair NIS, Airan RD, Bettgowda C, Rosch KS, Qin Q, van Zijl PCMV, Pillai JJ, Hua J (2020) Whole-brain functional and diffusion tensor MRI in human participants with metallic orthodontic braces. *Radiology* 294:149–157.
- Nilssen ES, Doan TP, Nigro MJ, Ohara S, Witter MP (2019) Neurons and networks in the entorhinal cortex: a reappraisal of the lateral and medial entorhinal subdivisions mediating parallel cortical pathways. *Hippocampus* 29:1238–1254.

- Ogawa S, Menon RS, Tank DW, Kim SG, Merkle H, Ellermann JM, Ugurbil K (1993) Functional brain mapping by blood oxygenation level-dependent contrast magnetic resonance imaging. *J Biophys* 64:803–812.
- Price JL, Ko AI, Wade MJ, Tsou SK, McKeel DW, Morris JC (2001) Neuron number in the entorhinal cortex and CA1 in preclinical Alzheimer disease. *Arch Neurol* 58:1395–1402.
- Reagh ZM, Yassa MA (2014) Object and spatial mnemonic interference differentially engage lateral and medial entorhinal cortex in humans. *Proc Natl Acad Sci U S A* 111:E4264–E4273.
- Reagh ZM, Noche JA, Tustison NJ, Delisle D, Murray EA, Yassa MA (2018) Functional imbalance of anterolateral entorhinal cortex and hippocampal dentate/CA3 underlies age-related object pattern separation deficits. *Neuron* 97:1187–1198.e4.
- Schar M, Kozerke S, Fischer SE, Boesiger P (2004) Cardiac SSFP imaging at 3 Tesla. *Magn Reson Med* 51:799–806.
- Squire LR, Stark CE, Clark RE (2004) The medial temporal lobe. *Annu Rev Neurosci* 27:279–306.
- Teeuwisse WM, Brink WM, Webb AG (2012) Quantitative assessment of the effects of high-permittivity pads in 7 Tesla MRI of the brain. *Magn Reson Med* 67:1285–1293.
- Tran TT, Speck CL, Gallagher M, Bakker A (2021) Lateral entorhinal cortex dysfunction in amnesic mild cognitive impairment. *Neurobiol Aging* 112:151–160.
- Ugurbil K (2013) Pushing spatial and temporal resolution for functional and diffusion MRI in the Human Connectome Project. *Neuroimage* 80:80–104.
- Ugurbil K, Garwood M, Ellermann J, Hendrich K, Hinke R, Hu X, Kim SG, Menon R, Merkle H, Ogawa S (1993) Imaging at high magnetic fields: initial experiences at 4 T. *Magn Reson Q* 9:259–277.
- Van Hoesen GW, Hyman BT, Damasio AR (1991) Entorhinal cortex pathology in Alzheimer's disease. *Hippocampus* 1:1–8.
- van Strien NM, Cappaert NL, Witter MP (2009) The anatomy of memory: an interactive overview of the parahippocampal-hippocampal network. *Nat Rev Neurosci* 10:272–282.
- Wagstyl K, Larocque S, Cucurull G, Lepage C, Cohen JP, Bludau S, Palomero-Gallagher N, Lewis LB, Funck T, Spitzer H, Dickscheid T, Fletcher PC, Romero A, Zilles K, Amunts K, Bengio Y, Evans AC (2020) BigBrain 3D atlas of cortical layers: cortical and laminar thickness gradients diverge in sensory and motor cortices. *PLoS Biol* 18:e3000678.
- Witter MP, Moser EI (2006) Spatial representation and the architecture of the entorhinal cortex. *Trends Neurosci* 29:671–678.
- Yassa MA, Stark SM, Bakker A, Albert MS, Gallagher M, Stark CE (2010) High-resolution structural and functional MRI of hippocampal CA3 and dentate gyrus in patients with amnesic mild cognitive impairment. *Neuroimage* 51:1242–1252.
- Yeung LK, Olsen RK, Bild-Enkin HEP, D'Angelo MC, Kacollja A, McQuiggan DA, Keshabyan A, Ryan JD, Barense MD (2017) Anterolateral entorhinal cortex volume predicted by altered intra-item configural processing. *J Neurosci* 37:5527–5538.
- Yushkevich PA, Piven J, Hazlett HC, Smith RG, Ho S, Gee JC, Gerig G (2006) User-guided 3D active contour segmentation of anatomical structures: significantly improved efficiency and reliability. *Neuroimage* 31:1116–1128.